

Observation of Proton-Coupled Electron Transfer by Transient Absorption Spectroscopy in a Hydrogen-Bonded, Porphyrin Donor–Acceptor Assembly

Niels H. Damrauer, Justin M. Hodgkiss, Joel Rosenthal, and Daniel G. Nocera*

Department of Chemistry, 6-335, Massachusetts Institute of Technology, 77 Massachusetts Avenue, Cambridge, Massachusetts 02139-4307

Received: February 16, 2004

Proton-coupled electron transfer (PCET) kinetics of a Zn(II) porphyrin donor noncovalently bound to a naphthalene-diimide acceptor through an amidinium-carboxylate interface have been investigated by time-resolved spectroscopy. The S_1 singlet excited-state of a Zn(II) 2-amidinium-5,10,15,20-tetramesitylporphyrin chloride ($ZnP\text{-}\beta\text{-AmH}^+$) donor is sufficiently energetic (2.04 eV) to reduce a carboxylate-diimide acceptor ($\Delta G^\circ = -460$ mV, THF). Static quenching of the porphyrin fluorescence is observed and time-resolved measurements reveal more than a 3-fold reduction in the S_1 lifetime of the porphyrin upon amidinium-carboxylate formation (THF, 298 K). Picosecond transient absorption spectra of the free $ZnP\text{-}\beta\text{-AmH}^+$ in THF reveal the existence of an excited-state isosbestic point between the S_1 and T_1 states at $\lambda_{\text{probe}} = 650$ nm, providing an effective ‘zero-kinetics’ background on which to observe the formation of PCET photoproducts. Distinct rise and decay kinetics are attributed to the build-up and subsequent loss of intermediates resulting from a forward and reverse PCET reaction, respectively ($k_{\text{PCET}}(\text{fwd}) = 9 \times 10^8 \text{ s}^{-1}$ and $k_{\text{PCET}}(\text{rev}) = 14 \times 10^8 \text{ s}^{-1}$). The forward rate constant is nearly 2 orders of magnitude slower than that measured for covalently linked Zn(II) porphyrin–acceptor dyads of comparable driving force and D–A distance, establishing the importance of a proximal proton network in controlling charge transport.

Introduction

Proton-coupled electron transfer (PCET) was launched as a mechanistic field of study with the synthesis of donor–acceptor (D–A) pairs assembled by hydrogen-bonding interfaces ($[H^+]$).^{1–3} Initial D– $[H^+]$ –A assemblies employed dicarboxylic acid dimers,^{4,5} Watson–Crick base pairs^{6,7} and related $[H^+]$ interfaces.⁸ Because charge redistribution within these interfaces is negligible, the presence of the proton network has little effect on the ET rate; the only available mechanism for PCET arises from the small dependence of the electronic coupling on the proton coordinate within the interface.⁹ Nonetheless, such cases are unusual in nature where proton displacement within a proximal network often strongly influences ET.^{2,10} For instance, ET between oxygen-evolving complex and the primary chlorophyll P680 of Photosystem II is governed by proton transfer of an intervening tyrosine (Y_Z), which is connected to a proton-transfer network via a histidine (D1-H190).¹¹ In cytochrome *c* oxidase, ET between the binuclear copper center and heme *a* is proton-controlled by an essential glutamate (E286)^{12,13} as is the redox activation of oxygen at heme *a*₃ by a proximal tyrosine, (Y288).^{14,15} We have shown that the control exerted by proximal proton-transfer networks on ET and oxygen bond activation events may be captured in D– $[H^+]$ –A assemblies possessing $[H^+]$ interfaces capable of supporting proton transfer. The pronounced effect of a proton-transfer network on catalytic O–O bond activation has been inferred from reactivity studies of redox cofactors appended with properly oriented $[H^+]$ interfaces.^{16,17} Its effect on charge transfer has been inferred from the excited state decay of the photoexcited donor of D– $[H^+]$ –[salt-bridge]–A assemblies.^{18–22} In no case, however, have reaction

kinetics been ascertained directly from observed intermediates of these types of tightly coupled PCET assemblies.

The challenge to directly measuring PCET kinetics by transient absorption spectroscopy arises as a direct consequence of the presence of a proton transfer network proximal to the electron transfer network. In tightly coupled networks, the proton significantly retards the ET rate so that charge transport is slow with respect to the dynamics of a photoexcited donor. Most notably for porphyrin donors, significant optical intensities associated with S_1 and T_1 excited state interconversions overwhelm the optical signatures of PCET intermediates. Accordingly, measurement of charge transport in tightly coupled PCET networks has been confined to monitoring the disappearance of the S_1 excited state by transient emission or absorption spectroscopy. However, this approach can be problematic because the dynamics of luminescence decay are not necessarily specific to charge transport and PCET does not always proceed from the emitting state. With regard to this latter issue, transient EPR experiments of PCET assemblies involving porphyrins have established the viability of the excited state donor to be T_1 as opposed to S_1 .²³ In light of these complications, specific to studies of tightly coupled PCET networks, it is desirable to develop approaches that enable PCET kinetics to be determined from directly observed charge transport intermediates. We now report such an approach for a PCET network composed of a porphyrin donor bridged to a diimide acceptor via an amidinium-carboxylate salt bridge.

Experimental Section

Materials. Silica gel 60 (70–230 and 230–400 mesh, Merck) and Merck 60 F254 silica gel (Precoated sheets, 0.2 mm thick) were used for column and analytical thin-layer chromatography,

respectively. Solvents for synthesis were of reagent grade or better and were dried according to standard methods.²⁴ Spectroscopic experiments employed CH₂Cl₂ and THF (spectroscopic grade, Burdick & Jackson) which were dried using standard methods and stored under high-vacuum. All other reagents were used as received. ¹H NMR spectra were collected in CDCl₃ or THF-*d*₈ (Cambridge Isotope Laboratories) using either a Mercury 300 or an Inova 500 spectrometer at 25 °C. All chemical shifts are reported using the standard δ notation in parts-per-million. Mass spectral and NMR analyses were performed in the MIT Department of Chemistry Instrumentation Facility (DCIF). Porphyrin **1** was prepared using previously reported procedures.²⁵

Synthesis of [N-(2,5-Di-*tert*-butylphenyl)-N'-(4-carboxyphenyl)naphthalene-1,8:4,5-tetracarboxydiimide][TMA] (2**).** A solution of 1,8:4,5-naphthalenedianhydride (5.0 g, 18.64 mmol), 4-aminobenzoate (2.55 g, 18.64 mmol) and 2,5-di-*tert*-butylaniline (3.83 g, 18.64 mmol) in DMF (100 mL) was refluxed under a nitrogen atmosphere for 16 h. The solution was then cooled to 0 °C and *N,N'*-(2,5-di-*tert*-butylphenyl)-1,8:4,5-naphthalenetetracarboxydiimide was removed as a side product by filtration and washed with cold CH₂Cl₂. The filtrate was concentrated under reduced pressure, redissolved in CH₂Cl₂ and washed with 5% HCl. The organic layer was then separated, and the aqueous layer was extracted twice with 100 mL of CH₂Cl₂. The organic layers were combined, dried over Na₂SO₄ and concentrated under reduced pressure. The resultant residue was chromatographed on silica gel, eluting with CH₂Cl₂ to remove nonpolar impurities and then with CH₂Cl₂ and MeOH (75:1 v:v) to give the desired product, which was recrystallized from CH₂Cl₂ and hexanes. The purified product was filtered and washed with cold CH₂Cl₂ and hexanes (1:3 v:v) to afford the pure carboxylic acid diimide in 12% yield (1.28 g). ¹H NMR (300 MHz, CDCl₃, 25 °C) 8.89 (s, 4H), 8.36 (d, *J* = 8.1 Hz, 2H), 7.63 (d, *J* = 8.7 Hz, 1H), 7.51 (dd, *J*₁ = 8.7 Hz; *J*₂ = 2.4 Hz, 1H), 7.50 (d, *J* = 8.1 Hz, 2H), 7.04 (d, *J* = 2.4 Hz, 1H), 1.35 (s, 9H), 1.29 (s, 9H). ESI-MS (MNa⁺) for C₃₆H₃₃N₂O₆Na, *m/z*: calcd 597.20, found 597.20.

The carboxylic diimide was converted to the corresponding carboxylate salt by dissolving 123 mg (0.214 mmol) of the acceptor in 25 mL of 2% MeOH in CH₂Cl₂ and cooling the resultant solution to -78 °C. In dropwise fashion, 90.1 μ L of tetramethylammonium hydroxide (TMAOH) (25% in MeOH) was added to the cold stirring solution, which was stirred for an additional 5 min at -78 °C and then warmed to room temperature. Concentration of the solution under reduced pressure yielded a solid, which was dried for 14 h under vacuum. A pure product was obtained in quantitative yield. ¹H NMR (300 MHz, CDCl₃, 25 °C) 8.78 (b, 4H), 8.24 (d, *J* = 8.4 Hz, 2H), 7.56 (d, *J* = 8.7 Hz, 1H), 7.47 (dd, *J*₁ = 8.7 Hz; *J*₂ = 2.1 Hz, 1H), 7.26 (d, *J* = 8.4 Hz, 2H), 7.00 (d, *J* = 2.1 Hz, 1H), 3.33 (s, 12H), 1.30 (s, 9H), 1.23 (s, 9H). ESI-MS ([M - N(CH₃)₄ + 2H⁺]) for C₃₆H₃₄N₂O₆, *m/z*: calcd 575.22, found 575.22.

Synthesis of [N-(2,5-Di-*tert*-butylphenyl)-N'-(carboxymethyl)naphthalene-1,8:4,5-tetracarboxydiimide][TMA] (3**).** Preparation of the methylene-spaced carboxylic acid naphthalene diimide acceptor was analogous to the foregoing synthesis of **2**, except that glycine was used in place of 4-aminobenzoate. ¹H NMR (300 MHz, CDCl₃, 25 °C) 8.83 (b, 4H), 7.60 (d, *J* = 5.4 Hz, 1H), 7.49 (dd, *J*₁ = 3.6 Hz; *J*₂ = 1.5 Hz, 1H), 7.00 (d, *J* = 1.2 Hz, 1H), 5.01 (s, 2H), 1.31 (s, 9H), 1.25 (s, 9H). ESIMS (MH⁺) for C₃₀H₃₀N₂O₆, *m/z*: calcd 513.20, found 513.20.

Deprotonation of the methylene spaced carboxylic diimide

was accomplished in a manner identical to that for **2**. ¹H NMR (300 MHz, CDCl₃, 25 °C) 8.72 (b, 4H), 7.58 (d, *J* = 3.3 Hz, 1H), 7.46 (dd, *J*₁ = 4.0 Hz; *J*₂ = 1.1 Hz, 1H), 7.00 (d, *J* = 1.0 Hz, 1H), 4.73 (s, 2H), 3.35 (b, 12H), 1.31 (s, 9H), 1.27 (s, 9H). ESIMS ([M - N(CH₃)₄ + 2H⁺]) for C₃₀H₃₀N₂O₆, *m/z*: calcd 513.20, found 513.20.

Physical Methods. Samples for steady-state spectroscopic measurements were contained within high-vacuum cells consisting of a 1 cm path length clear fused-quartz cell, which was connected to a 10-cm³ solvent reservoir via a graded seal. The two chambers were isolated from the environment and from each other by high-vacuum Teflon valves. An aliquot of **1** was added to the high-vacuum cell and an initial aliquot of diimide acceptor was added to the solvent reservoir. The transferring solvent was removed from both compartments on a high vacuum manifold (<10⁻⁵ Torr). Dry THF was added to the cell by vacuum transfer to make a 25 μ M solution of **1**. In this configuration, spectroscopy on **1** was examined initially. Then, by opening the valve between the two compartments, **1** was mixed with the diimide acceptor to form the associated complex while maintaining high vacuum and exactly the same amount of solvent and compound. After each measurement, the solution was transferred to the high-vacuum cell and isolated from the solvent reservoir by closing the high-vacuum Teflon valve. The solvent reservoir was then reopened and charged with an additional aliquot of the diimide; each time the transferring solvent was removed under high vacuum, after which it was mixed with the solution contained in the high vacuum cell. All spectroscopy was performed at 298 K.

In the case of assembly **1:3**, *K_a* was determined from luminescence quenching of the S₁ excited state as **3** was added to solution. Steady-state fluorescence spectra were recorded on an automated Photon Technology International QM 4 fluorometer that is equipped with a 150-W Xe arc lamp and a Hamamatsu R928 photomultiplier tube. In this experiment the excitation wavelength was 560 nm and emission was collected from 580 to 720 nm. Association constants (*K_a*) were determined from Benesi-Hildebrand plots of the luminescence intensity as a function of carboxylate concentration where the asymptotic fluorescence intensity limit was obtained for **3** in a large excess.²⁶

Electrochemical experiments were carried out using a Bio-analytical Systems (BAS) Model CV-50W potentiostat/galvanostat. Cyclic voltammetry was performed in a two-compartment cell using a platinum disk as the working electrode, a Ag/AgCl reference electrode, and a platinum wire auxiliary electrode. The supporting electrolyte used for electrochemistry experiments was either 0.1 M *n*-tetrabutylammonium hexafluorophosphate (TBAPF₆) or perchlorate (TBAP). The solution in the working compartment of the cell was deaerated by a nitrogen stream. Background cyclic voltammograms of the electrolyte solution were recorded prior to addition of the solid sample. Redox couples were referenced to SCE by using a ferricenium-ferrocene internal standard of 0.307 V vs SCE.²⁷

Spectroelectrochemical studies were performed in an optically transparent 1 mm thin-layer cell using a platinum mesh working electrode, a Ag/AgCl reference electrode, and a platinum wire auxiliary electrode. The supporting electrolyte used was 0.1 M TBAPF₆ in THF. Oxidation was carried out at 1200 mV versus the reference electrode and absorption spectra were recorded at selected time intervals. Extinction coefficients for the oxidized porphyrin (**1**⁺) were calculated based on the disappearance of initial porphyrin absorbance. Comparison of the spectra for **1** before the oxidation process and after a short recovery period

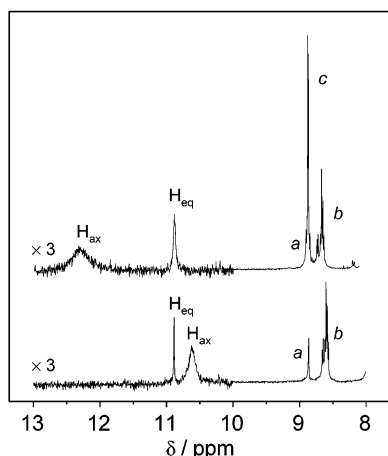


Figure 1. ^1H NMR spectra of the Ni(II) derivative of **1** (bottom) and associated to **3** (top) in THF- d_8 . The displayed spectral range captures the amidinium protons internal (NH_{ax}) and external (NH_{eq}) to the salt bridge interface. Labels (a) and (b) represent the resonances of the β -pyrrole protons adjacent to and distal from the amidinium functionality, respectively. The large resonance labeled (c) corresponds to the aromatic naphthalene protons of **3**. Resonances (a) and (b) display negligible shifts upon amidinium–carboxylate binding to form the supramolecular complex.

constancy of their chemical shift with supramolecular formation indicates that that π -stacking is not an important association mechanism. DFT calculations of the supramolecular complex support this contention. Energy optimized geometry calculations confirms association via the two-point hydrogen bond (Figure S1); a π -stacked complex was not observed. Moreover, geometry optimization shows that there is no opportunity for the acceptor to achieve face-to-face contact with the donor while maintaining the two-point hydrogen bond. The geometry optimized structure shows one other notable feature—the amidinium is rotated by $\sim 76^\circ$ with respect to the porphyrin macrocycle. This canting leads to the electronic decoupling of the amidinium functionality from the porphyrin chromophore. Consequently, the absorption spectrum of **1** in THF, typical of a standard Zn(II) porphyrin four-orbital model ($\lambda_{\text{abs,max}}(\text{B}) = 428 \text{ nm}$ ($\epsilon = 4.0 \times 10^4 \text{ M}^{-1} \text{ cm}^{-1}$); $\lambda_{\text{abs,max}}(\text{Q}_{1,0}) = 562 \text{ nm}$ ($\epsilon = 1.4 \times 10^4 \text{ M}^{-1} \text{ cm}^{-1}$); $\lambda_{\text{abs,max}}(\text{Q}_{0,0}) = 601 \text{ nm}$ ($\epsilon = 6.8 \times 10^3 \text{ M}^{-1} \text{ cm}^{-1}$)), is not perturbed upon association of the amidinium to the carboxylate acceptors. Owing to the insensitivity of these spectral features to the protonation state of the amidinium, we are only afforded optical signatures pertinent to the electron-transfer component of the PCET reaction.

There exists a -500 mV driving force for electron transfer from the singlet excited state (S_1) to the diimide acceptor of the **1:2** complex.³⁸ Nonetheless, PCET is not observed. Electronic excitation of **1** affords S_1 luminescence ($\lambda_{\text{em,max}}(\text{Q}_{0,0}) = 612 \text{ nm}$ and $\lambda_{\text{em,max}}(\text{Q}_{1,0}) = 665 \text{ nm}$), which is not quenched upon titration of 0–12 equivalents of **2** per equivalent of **1**. Conversely, time-resolved emission experiments show that the S_1 lifetime monotonically increases from 2.19 ns (THF, 298 K) for unbound **1** to 2.3 ns for **1:2**. This result is comparable to the lifetime increase observed when **1** is titrated with benzoate, a base that binds but cannot be reduced. Transient absorption measurements of the **1:2** complex reveal that the S_1 excited-state relaxes to the triplet excited state (T_1) with the normal intersystem-crossing rate of $k_{\text{isc}} = (4.3 \pm 0.6) \times 10^8 \text{ s}^{-1}$. A 450 mV decrease in reducing power accompanies this relaxation to T_1 ,³⁹ thereby precluding PCET from occurring. Thus, charge transport from S_1 is too slow to compete with $T_1 \leftarrow S_1$ intersystem crossing. The proton-network retards charge trans-

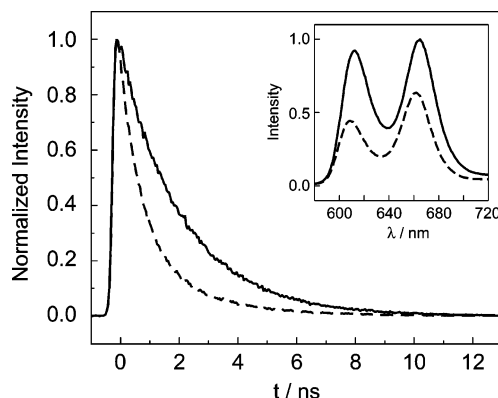


Figure 2. Singlet (S_1) emission kinetics for a $6 \times 10^{-5} \text{ M}$ solution of **1** in THF (solid) and in the presence of two equivalents of **3** (dashed). The inset shows static quenching of the emission spectrum for **1** (solid) ($2.5 \times 10^{-5} \text{ M}$) upon addition of three equivalents of **3** (dashed).

port to such a degree that it cannot effectively compete with the internal relaxation dynamics of the electronically excited porphyrin donor.

Replacement of the phenylene spacer with a methylene group results in a considerable shortening of the edge-to-edge through bond distance while maintaining a comparable driving force for a PCET reaction (-460 mV).³⁸ Under these conditions, the S_1 emission of porphyrin **1** in THF is quenched upon its association to **3**; static quenching of the S_1 fluorescence of **1** by $\sim 40\%$ is observed in the limit of salt-bridge formation (Figure 2 inset). The K_a for the **1:3** complex may be determined from the concentration dependence of this luminescence quenching. A Benesi–Hildebrand fit of the intensity of the S_1 luminescence band with added carboxylate yields $K_a(\mathbf{1:3}) = (2.4 \pm 0.6) \times 10^4$. A time-resolved fluorescence decay trace of the quenching process is shown in Figure 2. Compound **1** exhibits single-exponential decay kinetics with an observed lifetime of $\tau_{\text{obs}}(\mathbf{1}) = 2.19 \pm 0.07 \text{ ns}$ (298 K, THF), corresponding directly to the lifetime of the S_1 state. A marked decrease in lifetime of the S_1 state is observed and decay traces become biexponential upon **1:3** formation. The minor decay component corresponds to the excited-state relaxation of unbound species **1** and the major decay component is attributed to a quenched S_1 excited state of **1** associated to **3** ($\tau_{\text{obs}}(\mathbf{1:3}) = 0.72 \pm 0.03 \text{ ns}$). A quantitative analysis of the ratio of these two components leads to an alternative measure of $K_a(\mathbf{1:3}) = (2.8 \pm 0.6) \times 10^4$, which is consistent with the result obtained from the steady-state titration described above.⁴⁰ The quenching rate is found to be $(9.5 \pm 0.6) \times 10^8 \text{ s}^{-1}$ ($k = 1/\tau_{\text{obs}}(\mathbf{1:3}) - 1/\tau_{\text{obs}}(\mathbf{1:benzoate})$). This calculation employs the natural lifetime of **1** bound to benzoate ($\tau_0 = 2.3 \text{ ns}$) since, as mentioned above, the S_1 lifetime is slightly perturbed by salt-bridge formation, even in the absence of a redox-inactive quencher.

Transient absorption spectroscopy was undertaken with the aim of defining the quenching mechanism within the **1:3** complex. For these studies, THF was chosen as the solvent because of its ability to axially bind the Zn(II) center of **1**, thereby inhibiting molecular aggregation at the relatively high concentrations needed to acquire transient absorption spectra.⁴¹ Figure 3 shows transient absorption spectra of **1** at 500 ps, 1 ns and 2 ns following laser excitation. The 500 ps spectrum consists of broad transient absorption of the S_1 porphyrin excited state that dominates the visible spectral region.⁴² Superimposed on this absorption envelope are two prominent bleach features at 562 and 602 nm, corresponding to loss of ground-state Q-band absorptions. As shown in Figure 4a (solid circles), the TA signal of S_1 at 615 nm decays with a rate constant of $4.6 \times 10^8 \text{ s}^{-1}$;

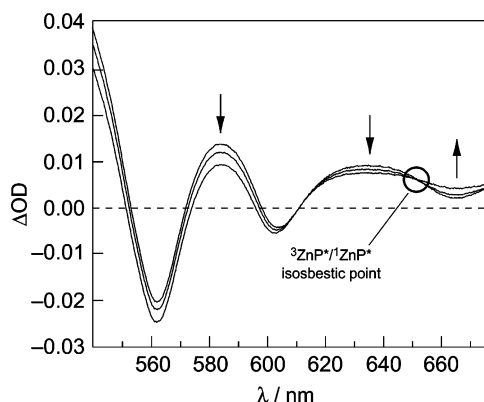


Figure 3. Pump-probe transient spectra of **1** (50 μM) in THF at 298 K collected at 500 ps, 1 ns, and 2 ns.

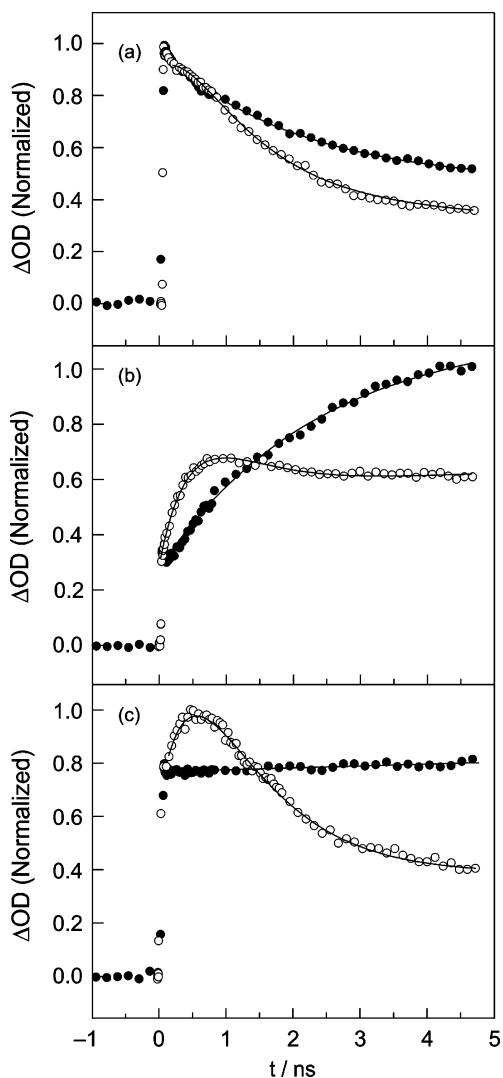


Figure 4. Pump-probe kinetics for **1** (solid circles) and **1:3** (open circles) probed at (a) 615 nm, (b) 660 nm and (c) the S_1 - T_1 isosbestic point at 650 nm. The supramolecular complex was formed from addition of two equivalents of **3** to **1** (50 μM) in THF. Fits to the data are shown by solid lines. See text for details of the fitting procedure.

previous studies of Zn(II) porphyrins shows that this decay is predominantly due to intersystem crossing to the T_1 excited state.⁴² Unfortunately, the TA features associated with these S_1 dynamics overlap with the optical signatures of the PCET products; spectroelectrochemical measurements of the porphyrin cation radical yields $\lambda_{\text{max}} = 412$ and 637 nm and the radical

anion of the diimide is known to absorb at $\lambda_{\text{max}} = 475$ and 610 nm.⁴³ Because the quenching process is in kinetic competition with intersystem crossing and the optical signatures for the S_1 and T_1 excited states are strong, the transient signals of the charge separated intermediates are overwhelmed. This can be observed from the decay trace of the transient signal of the **1:3** complex at 615 nm (open circles, Figure 4a). The overall transient decay for **1** is accelerated in the presence of **3**, and the yield of T_1 is attenuated, consistent with a quenching process. But rise and decay associated with charge separation and recombination is not clearly discernible; rather a weak shoulder at early times in the decay trace is observed.

We attempted to minimize the contribution of $T_1 \leftarrow S_1$ dynamics to the transient signal by moving to longer wavelengths, where the S_1 and T_1 absorbance is weaker. However, the transient spectrum at $\lambda > 650$ nm is complicated by S_1 stimulated emission. S_1 stimulated emission leads to an increased photon flux at the detector. This is manifested in an apparent decrease in the absorption of the S_1 . Consequently, as shown in Figure 4b (solid circles), a rise in ΔOD at $\lambda_{\text{probe}} = 660$ nm is observed as S_1 is lost and T_1 is formed. We note that the intensity of the stimulated emission is governed by the S_1 population. Hence, the growth of the TA signal in 4b occurs with the same kinetics as the disappearance of the TA signal in Figure 4a ($k_{\text{obs}} = (4.6 \pm 0.6) \times 10^8 \text{ s}^{-1}$). Owing to the smaller absorbance of the S_1 and T_1 excited states in this redder spectral region, transient signals of the Zn(II) porphyrin cation radical ($\epsilon_{660} = 2750 \text{ M}^{-1} \text{ cm}^{-1}$) are more pronounced upon the formation of the **1:3** complex. A rise and decay of the transient signal (open circles) is now clearly observed. However, the analysis is complicated by the superposition of the TA signals for the forward and reverse charge-transfer events within the **1:3** complex on the rising TA signal of **1**.

The PCET dynamics of **1:3** are greatly simplified when they are probed at the specific wavelength of 650 nm. The combination of rise and decay of ΔOD at the same rate results in an isosbestic point at 650 nm. Because the transient absorption spectrum of **1** at 650 nm does not change as a function of time, kinetics collected on **1** at this wavelength appear as a step function as shown in Figure 4c (solid circles). For our purposes, this steplike behavior of the transient absorption profile of **1** is extremely useful for two reasons. First, it provides a kinetics-free or flat background on which to examine PCET product formation in **1:3**. Second, we are afforded the fortunate situation that the porphyrin cation radical, formed as a result of PCET, has significant intensity at this wavelength ($\Delta\epsilon_{650} \approx 3000 \text{ M}^{-1} \text{ cm}^{-1}$).⁴⁴

Pump-probe kinetics collected for **1:3** at 650 nm are shown in Figure 4c (open circles). In contrast to the featureless transient collected for **1**, the time profile of **1:3** shows a prominent rise in ΔOD followed by subsequent decay corresponding to the appearance and disappearance, respectively, of the porphyrin cation radical. Quantitatively, PCET rate constants can be determined from a model that accounts for the kinetics of S_1 , T_1 , and the PCET photoproduct. The trace in Figure 4c was fit (solid line) by a sum of two variable exponentials with rate constants ($k_{\text{isc}} + k_{\text{PCET}}(\text{fwd})$) and $k_{\text{PCET}}(\text{rev})$ (where $k_{\text{PCET}}(\text{rev})$ refers to the rate constant with which ground state is reformed as a result of back PCET); intersystem crossing dynamics for unbound porphyrin species in the sample cell can be ignored as they do not contribute to the temporal change of ΔOD at this wavelength. This analysis yields forward and reverse PCET rates constants of $k_{\text{PCET}}(\text{fwd}) = (9 \pm 1) \times 10^8 \text{ s}^{-1}$ and $k_{\text{PCET}}(\text{rev}) = (14 \pm 1) \times 10^8 \text{ s}^{-1}$, respectively. It is noted that the

forward PCET rate constant obtained from transient absorption measurements is in excellent agreement with quenching rate constant measured by time-resolved fluorescence (vide supra). This result establishes that PCET occurs exclusively from the S_1 porphyrin excited state. It is noteworthy that the forward PCET rate constants are nearly 2 orders of magnitude slower than that measured for covalently linked Zn(II) porphyrin–acceptor dyads of comparable driving force in solvents of comparable dielectric constant.^{45,46} Although these systems cannot be rigorously compared owing to possible differences in electronic coupling, the significant disparity between the D–A kinetics of covalent and salt-bridge networks speak directly to the pronounced effect that a proximal proton-transfer network can have in mediating electron-transfer events.

Concluding Remarks

The propensity of proton transfer networks to retard charge transfer rates has practical consequences for mechanistic studies of PCET reactions. Attenuated rates translate to low yields of PCET intermediates. For this reason, it has been difficult to measure PCET reaction kinetics directly by time-resolved methods. Charge transfer has only been observed across hydrogen-bonded interfaces in which charge redistribution is negligible.^{4,47} For the systems described here, the proton network strongly perturbs charge transport. In **1:2**, PCET is not observed; in **1:3**, PCET intermediates are spectrally uncovered only when the transient difference signal between S_1 and T_1 excited states is minimized. This procedure, which is similar to one previously exploited in studies of D–A dyads⁴⁸ and heme protein–protein complexes,⁴⁹ opens the door to a host of future experiments designed to directly monitor rates of electron transfer that are strongly coupled to proton motion.

In closing, the importance of a proton network in controlling ET rates is becoming more apparent as the structural details of biological systems are revealed.^{50–64} The foregoing results establish that this emerging principle in biological charge transport can be modeled and studied directly in D–[H⁺]-A systems featuring proton-transfer networks.

Acknowledgment. We thank Dr. Chen-Yu Yeh and Dr. Scott Miller for synthesis and initial experiments on **1:2**. N.H.D. gratefully acknowledges the NIH for support of a postdoctoral fellowship. J.R. thanks the Fannie and John Hertz Foundation for a pre-doctoral fellowship. We kindly thank O.T.P. This work was supported by a grant from the National Institutes of Health (GM 47274).

Supporting Information Available: Structure and xyz coordinates for the gas-phase density functional calculation of the **1:3** complex. This material is available free of charge via the Internet at <http://pubs.acs.org>.

References and Notes

- Chang, C. J.; Brown, J. D. K.; Chang, M. C. Y.; Baker, E. A.; Nocera, D. G. In *Electron Transfer in Chemistry*; Balzani, V., Ed.; Wiley-VCH: Weinheim, Germany, 2001; Vol. 3.2.4, pp 409–461.
- Cukier, R. I.; Nocera, D. G. *Annu. Rev. Phys. Chem.* **1998**, *49*, 337–369.
- Chang, C. J.; Chang, M. C. Y.; Damrauer, N. H.; Nocera, D. G. *Biochim. Biophys. Acta* **2003**, in press.
- Turró, C.; Chang, C. K.; Leroi, G. E.; Cukier, R. I.; Nocera, D. G. *J. Am. Chem. Soc.* **1992**, *114*, 4013–4015.
- de Rege, P. J. F.; Williams, S. A.; Therien, M. J. *Science* **1995**, *269*, 1409–1413.
- Sessler, J. L.; Wang, B.; Springs, S. L.; Brown, C. T. In *Comprehensive Supramolecular Chemistry*; Murakami, Y., Ed.; Pergamon Press: Oxford, 1996; Vol. 4; p 311–336 and references therein.
- Shafirovich, V. Y.; Courtney, S. H.; Ya, N.; Geacintov, N. E. *J. Am. Chem. Soc.* **1995**, *117*, 4920–4929.
- Ghaddar, T. H.; Castner, E. W.; Isied, S. S. *J. Am. Chem. Soc.* **2000**, *122*, 1233–1234.
- Cukier, E.; Daniels, S.; Vinson, E.; Cave, R. J. *J. Phys. Chem. A* **2002**, *106*, 11240–11247.
- Hammes-Schiffer, S. *Acc. Chem. Res.* **2001**, *34*, 273–281.
- Tommos, C.; Babcock, G. T. *Biochim. Biophys. Acta* **2000**, *1458*, 199–219.
- Äldelroth, P.; Karpefors, M.; Gilderson, G.; Tomson, F. L.; Gennis, R. B.; Brzezinski, P. *Biochim. Biophys. Acta* **2000**, *1459*, 533–539.
- Namslauer, A.; Aagaard, A.; Katsonouri, A.; Brzezinski, P. *Biochemistry* **2003**, *42*, 1488–1498.
- Karpefors, M.; Äldelroth, P.; Namslauer, A.; Zhen, Y.; Brzezinski, P. *Biochemistry* **2000**, *39*, 14 664–14 669.
- Gennis, R. B. *Biochim. Biophys. Acta* **1998**, *1365*, 241–248.
- Chang, C. J.; Chng, L. L.; Nocera, D. G. *J. Am. Chem. Soc.* **2003**, *125*, 1866–1876.
- Chng, L. L.; Chang, C. J.; Nocera, D. G. *Org. Lett.* **2003**, *5*, 2421–2424.
- Roberts, J. A.; Kirby, J. P.; Nocera, D. G. *J. Am. Chem. Soc.* **1995**, *117*, 8051–8052.
- Deng, Y. Q.; Roberts, J. A.; Peng, S. M.; Chang, C. K.; Nocera, D. G. *Angew. Chem., Int. Ed. Engl.* **1997**, *36*, 2124–2127.
- Roberts, J. A.; Kirby, J. P.; Wall, S. T.; Nocera, D. G. *Inorg. Chim. Acta* **1997**, *263*, 395–405.
- Kirby, J. P.; Vandantzig, N. A.; Chang, C. K.; Nocera, D. G. *Tetrahedron Lett.* **1995**, *36*, 3477–3480.
- Kirby, J. P.; Roberts, J. A.; Nocera, D. G. *J. Am. Chem. Soc.* **1997**, *119*, 9230–9236.
- Berman, A.; Izraeli, E. S.; Levanon, H.; Wang, B.; Sessler, J. L. *J. Am. Chem. Soc.* **1995**, *117*, 8252–8257.
- Armarego, W. L. F.; Perrin, D. D. *Purification of Laboratory Chemicals*, 4th ed.; Butterworth-Heinemann: Oxford, 1996.
- Yeh, C.-Y.; Miller, S. E.; Carpenter, S. D.; Nocera, D. G. *Inorg. Chem.* **2001**, *40*, 3643–3646.
- Connors, K. A. *Binding Constants*; Wiley: New York, 1987.
- Bard, A. J.; Faulkner, L. R. *Electrochemical Methods. Fundamentals and Applications*; John Wiley: New York, 1980.
- ADF2000.02, Vrije Universiteit Amsterdam: Amsterdam, The Netherlands, 1999.
- Te Velde, G.; Bickelhaupt, F. M.; Baerends, E. J.; Fonseca Guerra, C.; Van Gisbergen, S. J. A.; Snijders, J. G.; Ziegler, T. *J. Comput. Chem.* **2001**, *22*, 931–967.
- Becke, A. D. *Phys. Rev. A* **1988**, *38*, 3098–3100.
- Lee, C.; Yang, W.; Parr, R. G. *Phys. Rev. B* **1988**, *37*, 785–789.
- Van Lenthe, E.; Baerends, E. J.; Snijders, J. G. *J. Chem. Phys.* **1993**, *99*, 4597–4610.
- Van Lenthe, E.; Ehlers, A.; Baerends, E. J. *J. Chem. Phys.* **1999**, *110*, 8943–8953.
- Loh, Z.-H.; Miller, S. E.; Chang, C. J.; Carpenter, S. D.; Nocera, D. G. *J. Phys. Chem. A* **2002**, *106*, 11 700–11 708.
- Pranata, J.; Wierschke, S. G.; Jorgensen, W. L. *J. Am. Chem. Soc.* **1991**, *113*, 2810–2819.
- To assert the existence of a chemical equilibrium, the analytical response must be a nonlinear function of the ligand concentration (see Person, W. B. *J. Am. Chem. Soc.* **1965**, *87*, 167–170). This is most prominent when the equilibrium concentration of the bound complex is on the same order of magnitude as the concentration of the more dilute of the two unbound components. However, the high concentration conditions required for NMR spectroscopy on **1:3** mean that over 99% of **1** is bound, and the nonlinear region of the binding isotherm cannot be observed with any fidelity.
- Kobuke, Y.; Ogawa, K. *Bull. Chem. Soc. Jpn.* **2003**, *76*, 689–708.
- The S_1 excited-state of **1** in THF is 2.04 eV (298 K); cyclic voltammetry yields one-electron reduction potentials for amidinium porphyrin donor **1** and carboxylate diimide acceptor **2** of $E_{1/2}(1^{2+}/1) = 1060$ mV and $E_{1/2}(2^{-2-}) = -480$ mV vs Ag/AgCl in THF, respectively. The one-electron reduction potentials for carboxylate diimide acceptor **3** is $E_{1/2}(3^{-2-}) = -520$ mV vs Ag/AgCl in THF.
- Estimated based on the shifts in phosphorescence spectra compared with fluorescence spectra of related Zn porphyrins (see Gradyushko, A. T.; Tsvirko, M. P. *Opt. Spectrosc.* **1971**, *31*, 291–295).
- $K_a = Q(Q + 1)/([3]_0(Q + 1) - [1]_0Q)$, where Q is the ratio of the pre-exponential factors of the short (0.72 ns) and long (2.2 ns) components which also corresponds to the ratio $[1:3]/[1]$.
- In noncoordinating solvents such as CH_2Cl_2 , aggregation is observed as indicated by the appearance of a green solution, resulting from a shift in the Q-bands from 556 and 592 nm to 573 and 612 nm, respectively.
- Rodriguez, J.; Kirmaier, C.; Holten, D. *J. Am. Chem. Soc.* **1989**, *111*, 6500–6506.
- Rogers, J. E.; Kelly, L. A. *J. Am. Chem. Soc.* **1999**, *121*, 3854–3861.

(44) Neither the singlet (unpublished result) nor triplet (see ref 43) excited states of **3** exhibit absorption at 650 nm. These intermediates are the products of an energy transfer quenching mechanism, which in this case is not plausible: energy transfer from the porphyrin S_1 excited state to produce $^1\mathbf{3}^*$ is energetically uphill and the production of $^3\mathbf{3}^*$ is a spin-forbidden process.

(45) Wasielewski, M. R.; Niemczyk, M. P.; Svec, W. A.; Pewitt, E. B. *J. Am. Chem. Soc.* **1985**, *109*, 1080–1082.

(46) Osuka, A.; Yoneshima, R.; Shiratori, H.; Okada, S.; Taniguchi, S.; Mataga, N. *Chem. Commun.* **1998**, 1567–1568.

(47) Sessler, J. L.; Sathiosatham, M.; Brown, C. T.; Rhodes, T. A.; Wiederrecht, G. *J. Am. Chem. Soc.* **2001**, *123*, 3655–3660.

(48) Greenfield, S. R.; Svec, W. A.; Gosztola, D.; Wasielewski, M. R. *J. Am. Chem. Soc.* **1996**, *118*, 6767–6777.

(49) Liang, N.; Mauk, A. G.; Pielak, G. J.; Johnson, J. A.; Smith, M.; Hoffman, B. M. *Science* **1988**, *240*, 311–313.

(50) Stubbe, J.; Nocera, D. G.; Yee, C. S.; Chang, M. C. Y. *Chem. Rev.* **2003**, *103*, 2167–2201.

(51) Chang, M. C. Y.; Yee, C. S.; Stubbe, J.; Nocera, D. G. *Proc. Natl. Acad. Sci. U.S.A.* **2003**, submitted for publication.

(52) Yee, C. S.; Chang, M. C. Y.; Ge, J.; Nocera, D. G.; Stubbe, J. *J. Am. Chem. Soc.* **2003**, asap.

(53) Siegbahn, P. E. M.; Eriksson, L.; Himo, F.; Pavolv, M. *J. Phys. Chem. B* **1998**, *102*, 10 622–10 629.

(54) Carra, C.; Iordanova, N.; Hammes-Schiffer, S. *J. Am. Chem. Soc.* **2003**, *125*, 10 429–10 436.

(55) Westphal, K. L.; Tommos, C.; Cukier, R. I.; Babcock, G. T. *Curr. Opin. Plant Biol.* **2000**, *3*, 236–242.

(56) Tommos, C. *Philos. Trans. R. Soc. London B* **2002**, *357*, 1383–1394.

(57) Cukier, R. I.; Seibold, S. A. *J. Phys. Chem. B* **2002**, *106*, 12 031–12 044.

(58) Aubert, C.; Vos, M. H.; Mathis, P.; Eker, A. P. M.; Brettel, K. *Nature* **2000**, *405*, 586–590.

(59) Hille, R.; Anderson, R. F. *J. Biol. Chem.* **2001**, *276*, 31 193–31 201.

(60) Knapp, M. J.; Rickert, K.; Klinman, J. P. *J. Am. Chem. Soc.* **2002**, *124*, 3865–3874.

(61) Cohen, A.; Klinman, J. P. *Acc. Chem. Res.* **1998**, *31*, 397–404.

(62) Crofts, A. R.; Guergova-Kuras, M.; Kuras, R.; Ugulava, N.; Li, J. Y.; Hong, S. J. *Biochim. Biophys. Acta-Bioenerg.* **2000**, *1459*, 456–456.

(63) Berry, E. A.; Guergova-Kuras, M.; Huang, L.-S.; Crofts, A. R. *Annu. Rev. Biochem.* **2000**, *69*, 1005–1075.

(64) Graige, M. S.; Paddock, M. L.; Bruce, J. M.; Feher, G.; Okamura, M. Y. *J. Am. Chem. Soc.* **1996**, *118*, 9005–9016.